Inorg. Chem. **2005**, *44*, 2245–2254

Performance of Nonrelativistic and Quasi-Relativistic Hybrid DFT for the Prediction of Electric and Magnetic Hyperfine Parameters in ^{57}Fe Mössbauer Spectra

Sebastian Sinnecker, Leonardo D. Slep,† Eckhard Bill, and Frank Neese*

Max-Planck-Institut für Bioanorganische Chemie, Stiftstrasse 34-36, D-45470 Mülheim an der Ruhr, Germany

Received October 6, 2004

^{57}Fe electric and magnetic hyperfine parameters were calculated for a series of 10 iron model complexes, covering a wide range of oxidation and spin states. Employing the B3LYP hybrid method, results from nonrelativistic density functional theory (DFT) and quasi-relativistic DFT within the zero-order regular approximation (ZORA) were compared. Electron densities at the iron nuclei were calculated and correlated with experimental isomer shifts. It was shown that the fit parameters do not depend on a specific training set of iron complexes and are, therefore, more universal than might be expected. The nonrelativistic and quasi-relativistic electron densities gave fit parameters of similar quality; the ZORA densities are only shifted by a factor of 1.32, upward in the direction of the four-component Dirac–Fock value. From a correlation of calculated electric field gradients and experimental quadrupole splittings, the value of the ^{57}Fe nuclear quadrupole moment was redetermined to a value of 0.16 barn, in good agreement with other studies. The ZORA approach gave no additional improvement of the calculated quadrupole splittings in comparison to the nonrelativistic approach. The comparison of the calculated and measured ^{57}Fe isotropic hyperfine coupling constants (hfcc's) revealed that both the ZORA approach and the inclusion of spin–orbit contributions lead to better agreement between theory and experiment in comparison to the nonrelativistic results. For all iron complexes with small spin–orbit contributions (high-spin ferric and ferryl systems), a distinct underestimation of the isotropic hfcc's was found. Scaling factors of 1.81 (nonrelativistic DFT) and 1.69 (ZORA) are suggested. The calculated ^{57}Fe isotropic hfcc's of the remaining model systems (low-spin ferric and high-spin ferrous systems) contain 10–50% second-order contributions and were found to be in reasonable agreement with the experimental results. This is assumed to be the consequence of error cancellation because *g*-tensor calculations for these systems are of poor quality with the existing DFT approaches. Excellent agreement between theory and experiment was found for the ^{57}Fe anisotropic hfcc's. Finally, all of the obtained fit parameters were used for an application study of the $[Fe(H_2O)_6]^{3+}$ ion. The calculated spectroscopic data are in good agreement with the Mössbauer and electron paramagnetic resonance results discussed in detail in a forthcoming paper.

1. Introduction

Spectroscopic methods are essential tools for the elucidation of molecular geometries and electronic structures and provide a considerable number of parameters characterizing the investigated systems. Among them, Mössbauer (MB) parameters (the isomer shifts δ and the ^{57}Fe quadrupole splittings ΔE_Q) can be used as sensitive probes of the valence and spin states of ^{57}Fe-containing complexes.[1,2] The application of magnetic fields in MB experiments, or the use of electron paramagnetic resonance (EPR) methods,[3,4] additionally opens access to the spin-Hamiltonian parameters, for

* E-mail: neese@mpi-muelheim.mpg.de.
† Current address: Departamento de Química Inorgánica, Analítica y Química Física, INQUIMAE, Facultad de Ciencias Exactas y Naturales, Universidad de Buenos Aires, Pabellón 2, Ciudad Universitaria, C1428EHA Buenos Aires, Argentina.

(1) Gütlich, P.; Link, R.; Trautwein, A. *Mössbauer Spectroscopy and Transition Metal Chemistry*; Springer-Verlag: Heidelberg, Germany, 1978.
(2) Gonser, U. In *Mössbauer Spectroscopy*; Gonser, U., Ed.; Springer-Verlag: Berlin, 1975; pp 1−51.
(3) Weil, J. A.; Bolton, J. R.; Wertz, J. E. *Electron Paramagnetic Resonance − Elementary Theory and Practical Applications*; Wiley: New York, 1994.
(4) Schweiger, A.; Jeschke, G. *Principles of Pulse Electron Paramagnetic Resonance*; Oxford University Press: Oxford, U.K., 2001.

10.1021/ic048609e CCC: $30.25
Published on Web 02/26/2005

example, magnetic hyperfine coupling constants (hfcc's, A) and g-values as well as zero-field splitting (ZFS) parameters.[5,6] The availability of these data is often a key step in understanding the bonding situation in a given system and is of tremendous analytic value as well. The application of MB spectroscopy ranges from small inorganic ^{57}Fe complexes and minerals to metalloproteins and even whole cells.[7−9] It is also of great interest for the investigation of short-lived intermediates, where spectroscopy is the only source of information. From this point of view, theoretical studies of electric and magnetic hyperfine parameters can be very helpful for an interpretation of the measured spectroscopic data.[10−14]

In this work, electric and magnetic hyperfine parameters were calculated for 10 experimentally well-investigated mononuclear iron complexes, covering a wide range of oxidation numbers, spin states, and ligand types (Figure 1 and Table 1). Many of these complexes are unique in their class and present real synthetic achievements with far-reaching implications for the field of iron chemistry. However, in the present work, we will not touch upon the many issues associated with the molecules themselves but will focus on their spectroscopic properties. In this work, density functional theory (DFT)[15−17] is used to address the following issues: (i) How accurate are the calculated hyperfine parameters in comparison to those of the experiments? (ii) What is the influence of scalar relativistic corrections on the computed data? (iii) What is the best value of the ^{57}Fe nuclear quadrupole moment in conjunction with the methods employed in this work? The first two points are of essential importance for judging the accuracy of theoretical results that can be expected in application studies. The influence of scalar relativistic corrections was studied applying the zero-order regular approximation (ZORA).[18−20] The suitability of this method for the calculation of magnetic hfcc's was demonstrated in the pioneering work of van Lenthe and co-workers, employing a Slater-type orbital-based implementation.[21,22] In this study, the ZORA approach was used for the first time for the calculation of hfcc's in the framework of Gaussian-type orbitals. Our implementation is based on the work of van Wüllen and employs a model potential derived from atomic ZORA calculations for the

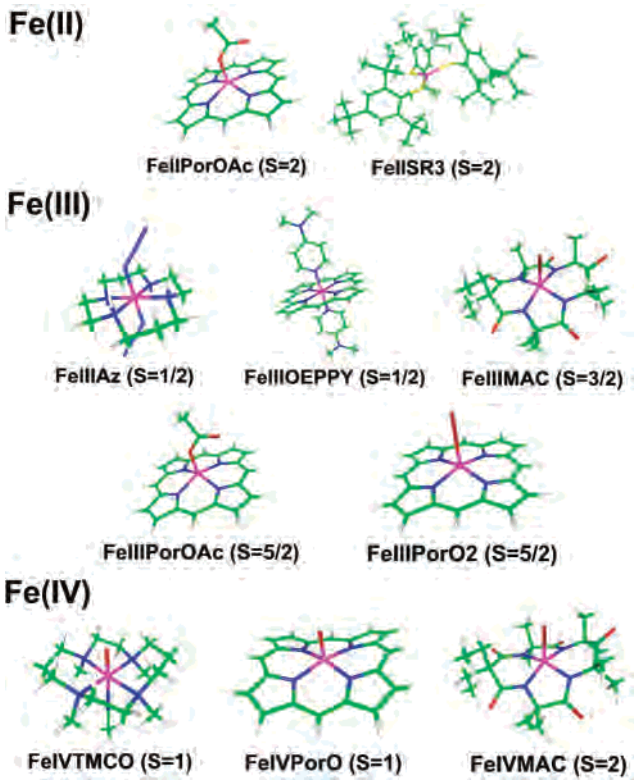

Figure 1. Investigated iron model complexes. Experimental results for Fe^{II}PorOAc were taken from $[Fe^{II}(CH_3CO_2)TPpivP]^-$ (Bominaar et al.),[26] for Fe^{II}SR3 from $[Ph_4P][Fe^{II}(SR)_3]\cdot 2MeCN\cdot C_7H_8$ with R=C_6H_2-2,4,6-tBu_3 (Sanakis et al. and MacDonnell et al.),[27,28] for Fe^{III}Az from *trans*-$[Fe^{III}(cyclam)(N_3)_2]ClO_4$ (Meyer et al.),[29] for Fe^{III}OEPPY from $[Fe(OEP)(4\text{-}NMe_2Py)_2]ClO_4$ (Safo et al.),[30] for Fe^{III}MAC from $[Et_4N]_2[Fe^{III}Cl(\eta^4\text{-}MAC^*)]\cdot CH_2Cl_2\cdot H_2O$ (Kostka et al.),[31] for Fe^{III}PorOAc from $[Fe^{III}(CH_3CO_2)\text{-}TPpivP]$ (Bominaar et al.),[26] for Fe^{III}PorO2 from $[Me_4N][Fe^{III}(OEP)O_2]$ (Burstyn et al.),[32] for Fe^{IV}TMCO from *trans*-$[Fe^{IV}(O)(TMC)(NCCH_3)]\text{-}(OTf)_2$ (Rohde et al.),[33] for Fe^{IV}PorO from $[Fe^{IV}(TMP)(O)]^+$ (Mandon et al.),[34] and for Fe^{IV}MAC from $[Et_4N][Fe^{IV}Cl(\eta^4\text{-}MAC^*)]$ (Kostka et al.).[31]

Table 1. Fe Oxidation States, Spin States, and Charges of the Investigated Model Systems (See Figure 1)

model system	Fe oxidation state	S_{Fe}	total charge
Fe^{II}PorOAc	II	2	−1
Fe^{II}SR3	II	2	−1
Fe^{III}Az	III	$^1/_2$	+1
Fe^{III}OEPPY	III	$^1/_2$	+1
Fe^{III}MAC	III	$^3/_2$	−2
Fe^{III}PorOAc	III	$^5/_2$	0
Fe^{III}PorO2	III	$^5/_2$	−1
Fe^{IV}TMCO	IV	1	+2
Fe^{IV}PorO[a]	IV	1	+1
Fe^{IV}MAC	IV	2	−1

[a] The metal is ferromagnetically coupled to a porphyrin $S = {}^1/_2$ radical (the entire spin is $S_t = {}^3/_2$).

(5) McWeeny, R. *Spins in Chemistry*; Academic Press: New York, 1970.
(6) Neese, F.; Solomon, E. I. In *Magnetism: Molecules to Materials*; Miller, J. S., Drillon, M., Eds. Wiley VCH: Weinheim, Germany, 2003; pp 345−466.
(7) Gütlich, P. In *Mössbauer Spectroscopy*; Gonser, U., Ed.; Springer-Verlag: Berlin, 1975; pp 53−96.
(8) Vrajmasu, V. V.; Bominaar, E. L.; Meyer, J.; Münck, E. *Inorg. Chem.* **2002**, *41*, 6358−6371.
(9) Johnson, C. E. In *Mössbauer Spectroscopy*; Gonser, U., Ed. Springer-Verlag: Berlin, 1975; pp 139−166.
(10) Han, W. G.; Lovell, T.; Liu, T. Q.; Noodleman, L. *Inorg. Chem.* **2004**, *43*, 613−621.
(11) Lovell, T.; Liu, T. Q.; Case, D. A.; Noodleman, L. *J. Am. Chem. Soc.* **2003**, *125*, 8377−8383.
(12) Zhang, Y.; Mao, J. H.; Oldfield, E. *J. Am. Chem. Soc.* **2002**, *124*, 7829−7839.
(13) Neese, F. *Inorg. Chim. Acta* **2002**, *337*, 181−192.
(14) Neese, F. *Curr. Opin. Chem. Biol.* **2003**, *7*, 125−135.
(15) Koch, W.; Holthausen, M. C. *A Chemist's Guide to Density Functional Theory*; Wiley-VCH: Weinheim, Germany, 2000.
(16) Kohn, W.; Sham, L. J. *Phys. Rev.* **1965**, *140*, 1133.
(17) Hohenberg, P.; Kohn, W. *Phys. Rev. B: Condens. Matter* **1964**, *136*, 864.
(18) van Lenthe, E.; Baerends, E. J.; Snijders, J. G. *J. Chem. Phys.* **1993**, *99*, 4597−4610.
(19) van Lenthe, E.; Baerends, E. J.; Snijders, J. G. *J. Chem. Phys.* **1994**, *101*, 9783−9792.
(20) van Lenthe, E.; van Leeuwen, R.; Baerends, E. J.; Snijders, J. G. *Int. J. Quantum Chem.* **1996**, *57*, 281−293.
(21) van Lenthe, E.; van der Avoird, A.; Wormer, P. E. S. *J. Chem. Phys.* **1998**, *108*, 4783−4796.
(22) Belanzoni, P.; van Lenthe, E.; Baerends, E. J. *J. Chem. Phys.* **2001**, *114*, 4421−4433.

solution of the ZORA equations.[23] The last point of interest (the redetermination of the ^{57}Fe nuclear quadrupole moment) contributes to a long-standing question in this area of research and is also important in order to achieve the best possible agreement between calculated and measured quadrupole splittings. Calculations are presently the only source of nuclear quadrupole moments because they cannot be directly measured nor can they presently be calculated with sufficient accuracy from nuclear structure theory.[24]

Finally, calculations on the high-spin iron complex $[Fe(H_2O)_6]^{3+}$ will be presented as an application case; that is, its spectroscopic data were computed employing the fit parameters, which were obtained for the model complexes in Table 1. Surprisingly, no high-quality experimental study on this fundamentally important species appears to be available and will, therefore, be reported in a forthcoming paper.[25]

2. Theory

The most important parameters available from MB studies are isomer shifts δ and quadrupole splittings ΔE_Q. δ is defined as the shift in γ-ray absorption energy relative to a given standard for the monitored ^{57}Fe $I = {}^1/_2 \rightarrow I = {}^3/_2$ nuclear spin transition of the absorber. This shift depends on the local environment of the iron nucleus in the absorber and was shown to be proportional to the electron density at the iron nucleus ρ_0.[1,2] For ^{57}Fe, a negative isomer shift indicates an increase in ρ_0 relative to the standard. In this work, the calculated ρ_0 values were plotted versus experimental isomer shifts and a linear regression was performed with the equation

$$\delta = \alpha(\rho_0 - C) + \beta \tag{1}$$

C is an arbitrary constant, which is introduced for convenience. The obtained fit parameters α and β can be used for the estimation of isomer shifts from calculated ρ_0 values. As noted previously, they noticeably depend on the employed density functionals and basis sets.[13,35] Consequently, each combination of basis set, functional, and relativistic treatment must be independently calibrated.

The second important quantity from MB studies, the quadrupole splitting ΔE_Q, is, likewise, a sensitive probe for the environment of the investigated metal center. It provides details of the asymmetry of the electron density in the vicinity of the MB atom. The ΔE_Q values can be calculated from the electric field gradients V_i ($i = x, y, z$) and the asymmetry parameter $\eta = (V_x - V_y)/V_z$:

$$\Delta E_{\mathrm{Q}} = \frac{1}{2} eQV_z \sqrt{1 + \frac{1}{3}\eta^2} \tag{2}$$

V_x, V_y, and V_z are the principal components of the electric field gradient tensors in a coordinate system with $|V_z| \geq |V_y| \geq |V_x|$, e is the electric charge of the positron, and $Q(^{57}\mathrm{Fe})$ is the nuclear quadrupole moment. Electric field gradients contain local contributions (e.g., from the iron orbitals) and lattice, bond, and three-center nonlocal contributions.[36] It is evident from eq 2 that an accurate value of $Q(^{57}\mathrm{Fe})$ must be known for the precise calculation of ΔE_Q. However, widely scattering values between 0.1 and 0.3 barn are found in the literature, depending on the level of theory used for the construction of the calibration curve.[14] As discussed by Schwerdtfeger et al., the best way to get an accurate determination of nuclear quadrupole moments is through the combination of accurately measured ΔE_Q values and precisely calculated electric field gradients.[24] This is also the strategy followed here. The electric field gradients obtained in this study were used for a redetermination of $Q(^{57}\mathrm{Fe})$ at the nonrelativistic and ZORA scalar relativistic levels of theory, employing eq 2 and the available experimental ΔE_Q values. In the nonrelativistic calculations, the field gradient at a nucleus A was simply evaluated as the expectation value of the field gradient operator $\hat{f}^A_{\mu\nu}$ ($\mu, \nu = x, y, z$) over the nonrelativistic density ρ with[37]

$$\hat{f}^A_{\mu\nu} = \frac{\partial^2}{\partial R_{A\mu} \partial R_{A\nu}} \left(\sum_i \frac{1}{|r_i - R_A|} - \sum_{J \neq A} \frac{Z_J}{|R_J - R_A|} \right) \tag{3}$$

Here, Z_J represents the nuclear charges and r_i and R_J denote electronic and nuclear position vectors, respectively. However, in the ZORA case, a more elaborate formalism is necessary, which has been discussed in detail by van Lenthe and Baerends.[38] Their suggestion was to replace the ZORA-SCF density with the so-called ZORA-4 density, which is supposed to introduce the small component density into the calculation. The ZORA-4 density ρ_i^{Z4} for each occupied

(23) van Wüllen, C. *J. Chem. Phys.* **1998**, *109*, 392−399.
(24) Schwerdtfeger, P.; Pernpointner, M.; Nazarewicz, W. In *Calculation of NMR and EPR Parameters. Theory and Applications*; Kaupp, M., Bühl, M., Malkin, V. G., Eds.; Wiley-VCH: Weinheim, Germany, 2004; pp 279−291.
(25) Bill, E.; Mienert, B.; Sinnecker, S.; Neese, F. Manuscript in preparation.
(26) Bominaar, E. L.; Ding, X. Q.; Gismelseed, A.; Bill, E.; Winkler, H.; Trautwein, A. X.; Nasri, H.; Fischer, J.; Weiss, R. *Inorg. Chem.* **1992**, *31*, 1845−1854.
(27) Sanakis, Y.; Power, P. P.; Stubna, A.; Münck, E. *Inorg. Chem.* **2002**, *41*, 2690−2696.
(28) MacDonnell, F. M.; Ruhlandtsenge, K.; Ellison, J. J.; Holm, R. H.; Power, P. P. *Inorg. Chem.* **1995**, *34*, 1815−1822.
(29) Meyer, K.; Bill, E.; Mienert, B.; Weyhermüller, T.; Wieghardt, K. *J. Am. Chem. Soc.* **1999**, *121*, 4859−4876.
(30) Safo, M. K.; Gupta, G. P.; Walker, F. A.; Scheidt, W. R. *J. Am. Chem. Soc.* **1991**, *113*, 5497−5510.
(31) Kostka, K. L.; Fox, B. G.; Hendrich, M. P.; Collins, T. J.; Rickard, C. E. F.; Wright, L. J.; Münck, E. *J. Am. Chem. Soc.* **1993**, *115*, 6746−6757.
(32) Burstyn, J. N.; Roe, J. A.; Miksztal, A. R.; Shaevitz, B. A.; Lang, G.; Valentine, J. S. *J. Am. Chem. Soc.* **1988**, *110*, 1382−1388.
(33) Rohde, J. U.; In, J. H.; Lim, M. H.; Brennessel, W. W.; Bukowski, M. R.; Stubna, A.; Münck, E.; Nam, W.; Que, L. *Science* **2003**, *299*, 1037−1039.
(34) Mandon, D.; Weiss, R.; Jayaraj, K.; Gold, A.; Terner, J.; Bill, E.; Trautwein, A. X. *Inorg. Chem.* **1992**, *31*, 4404−4409.
(35) Liu, T. Q.; Lovell, T.; Han, W. G.; Noodleman, L. *Inorg. Chem.* **2003**, *42*, 5244−5251.
(36) Serres, R. G.; Grapperhaus, C. A.; Bothe, E.; Bill, E.; Weyhermüller, T.; Neese, F.; Wieghardt, K. *J. Am. Chem. Soc.* **2004**, *126*, 5138−5153.
(37) Fowler, P. W.; Lazzeretti, P.; Steiner, E.; Zanasi, R. *Chem. Phys.* **1989**, *133*, 221−235.
(38) van Lenthe, E.; Jan Baerends, E. *J. Chem. Phys.* **2000**, *112*, 8279−8292.

molecular orbital ψ_i is defined as

$$\rho_i^{Z4} = \frac{\rho_i^Z + \rho_i^S}{1 + \langle\psi_i|Q[V_M]|\psi_i\rangle} \quad (4)$$

Here, ρ_i^Z is the ZORA-SCF density and ρ_i^S is the small component density. The scaling factor in the denominator is the expectation value of $Q[V]$ with respect to the molecular orbitals ψ_i, which is, in the scalar relativistic case,[19,38]

$$Q[V] = \mathbf{p}\frac{c^2}{(2c^2 - V_M)^2}\mathbf{p} \quad (5)$$

V_M is the model potential of van Wüllen,[23] and the one-electron ZORA density for the ith molecular orbital (MO) is defined as

$$\rho_i^Z(\mathbf{r}) = \psi_i^\dagger(\mathbf{r})\psi_i(\mathbf{r}) \quad (6)$$

Here, $\psi_i(\mathbf{r})$ represents the ZORA wave functions. In the scalar relativistic case, the small component density is defined as

$$\rho_i^s = \frac{c^2}{(2c^2 - V_M)^2}(\mathbf{p}\psi_i)^\dagger\mathbf{p}\psi_i \quad (7)$$

with the momentum $\mathbf{p} = -i\nabla$ and the velocity of light $c \approx 137$ in atomic units. In our ZORA implementation, the electric field gradient is calculated as the expectation value of the field gradient operator over ρ_i^{Z4}, precisely as it was suggested by van Lenthe and Baerends.[38]

If magnetic fields are applied in the MB experiments, the magnetic dipole splitting is revealed in addition to the electric quadrupole perturbation. From these data, the hyperfine tensor $A_{\mu\nu}$ of the ^{57}Fe center can be extracted, which describes the interaction between the nuclear magnetic moment and the unpaired electrons. $A_{\mu\nu}$ is a 3×3 matrix and consists of three parts: (i) the isotropic Fermi contact term A^F, (ii) the first-order traceless dipolar contribution $A_{\mu\nu}^D$, and (iii) the second-order nontraceless spin−orbit contribution (SOC) $A_{\mu\nu}^{orb}$ [39]

$$A_{\mu\nu} = \delta_{\mu\nu}A^F + A_{\mu\nu}^D + A_{\mu\nu}^{orb} \quad (8)$$

In this work, $^1/_3$ of the sum of the eigenvalues of the total hyperfine tensor will be referred to as the isotropic hfcc A^{iso}, which can therefore contain contributions from A^{orb}.

The nonrelativistic contributions i and ii were calculated in the usual way from the following expectation value:

$$A_{\mu\nu} = \frac{P_A}{2S}\int(\rho_\alpha - \rho_\beta)\left[3\frac{r_{\mu A}r_{\nu A}}{r_A^5} - \frac{\delta_{\mu\nu}}{r_A^3} + \frac{8\pi}{3}\delta(r_A)\,\delta_{\mu\nu}\right]\mathrm{d}^3r_A \quad (9)$$

P_A ($=g_e g_N \beta_e \beta_N$) is a factor of fundamental constants, containing the free electron g value g_e, the g value g_N of the magnetic nucleus A, the Bohr magneton β, and the nuclear magneton β_N. ρ_α and ρ_β are the spin densities. The dipolar hyperfine interaction is described by the first two terms, whereas the last term refers to the Fermi contact term. r_A is the position of the electron with respect to the position of nucleus A. In the ZORA framework, a more elaborate formalism is used that, again, is due to the pioneering work of van Lenthe and Baerends.[21] In this case, one obtains the matrix elements of the hfcc tensors in the scalar relativistic case from

$$A_{\mu\nu} = \frac{P_A}{2S}\int\frac{K}{r_A^3}[r_{\nu A}\nabla_\mu(\rho_\alpha - \rho_\beta) - \delta_{\mu\nu}r_A\nabla(\rho_\alpha - \rho_\beta)]\,\mathrm{d}^3r_A \quad (10)$$

which, in the nonrelativistic limit ($K = 1$), becomes eq 9. K is the ZORA specific relativistic correction in which the molecular potential V is replaced by the van Wüllens model potential V_M:

$$K = \frac{c^2}{c^2 - \frac{1}{2}V_M} \quad (11)$$

SOCs to the hyperfine tensors were calculated as second-order properties, employing the coupled perturbed (CP) Kohn−Sham theory:[39]

$$A_{\mu\nu}^{orb} = -\frac{P_A}{S}tr[Q_\mu^{(A)}h_\nu^{SOC}] \quad (12)$$

Here, $Q_\mu^{(A)}$ is the response spin density, obtained from the coupled perturbed Kohn−Sham equations with respect to a nuclear magnetic dipole perturbation, as explained in detail in ref 39. h_ν^{SOC} is an effective one-electron (effective nuclear charge or mean-field) approximation to the spin−orbit coupling operator ($\mu, \nu = x, y, z$).

3. Material and Methods

Ten experimentally well-investigated mononuclear iron complexes were selected from the literature. In the case of larger ligands, the side groups were truncated (e.g., substitution of tetramesitylporphyrin with porphyrin). The remaining model systems and the references to the experimental sources are given in Figure 1. Complete geometry optimizations were performed for all of the complexes, employing X-ray data as starting structures whenever possible. Furthermore, the structure of the $[Fe(H_2O)_6]^{3+}$ ion was geometry optimized. For these calculations, the pure density functional[15−17] BP[40−42] was used. The SV(P) basis set[43] was used for the main group elements together with the more accurate TZV(P) basis set for iron.[44]

Two single point calculations were performed for every optimized structure. In both cases, the B3LYP density functional[45−47] was used in combination with the CP(PPP) basis set for Fe[13] and

(39) Neese, F. *J. Chem. Phys.* **2003**, *118*, 3939−3948.
(40) Becke, A. D. *Phys. Rev. A: At., Mol., Opt. Phys.* **1988**, *38*, 3098−3100.
(41) Perdew, J. P. *Phys. Rev. B: Condens. Matter* **1986**, *34*, 7406.
(42) Perdew, J. P. *Phys. Rev. B: Condens. Matter* **1986**, *33*, 8822−8824.
(43) Schäfer, A.; Horn, H.; Ahlrichs, R. *J. Chem. Phys.* **1992**, *97*, 2571−2577.
(44) Schäfer, A.; Huber, C.; Ahlrichs, R. *J. Chem. Phys.* **1994**, *100*, 5829−5835.
(45) Becke, A. D. *J. Chem. Phys.* **1993**, *98*, 5648−5652.
(46) Lee, C. T.; Yang, W. T.; Parr, R. G. *Phys. Rev. B: Condens. Matter* **1988**, *37*, 785−789.
(47) Stephens, P. J.; Devlin, F. J.; Chabalowski, C. F.; Frisch, M. J. *J. Phys. Chem.* **1994**, *98*, 11623−11627.

the TZVP basis sets for oxygen, nitrogen, and chloride atoms directly attached to the metal.[44] The SV(P) basis sets were used for the remaining atoms.[43] Furthermore, the TZV/J (Fe, N, O, S) and SV/J (H, C) auxiliary basis sets[48,49] from the Turbomole 5.3 basis set library were employed.[50]

In the first single point calculation, a nonrelativistic SCF calculation was performed (labeled as NonRel) along with an additional calculation of SOCs to the iron hyperfine data (NonRel + SOC). For that purpose, a semiempirical one-electron SOC operator was used, employing the parametrization of Koseki et al.[51−53] The integration accuracy at the Fe centers was increased to 7. In the second set of calculations, scalar relativistic ZORA calculations were performed (labeled as ZORA). Here also, SOCs to the Fe hyperfine data were computed (ZORA + SOC).

In the ZORA calculations, all of the basis sets were completely decontracted in order to allow for an accurate response of the inner atomic shells to the relativistic potentials. The integration accuracy on the metal centers was increased to 14, and three steep s functions were added to the Fe CP(PPP) basis set.

The convergence of the Fe hyperfine tensors with respect to the number of steep s and p functions was tested in calculations on the Fe^{3+} high-spin ion. It was found that additional steep s or p functions change the calculated hyperfine data by less than 1 percent.

All of the calculations were performed employing the program package ORCA.[54] In this work, we present a first application of our new ZORA implementation for the calculation of magnetic and electric hyperfine data.[55]

4. Results and Analysis

Isomer Shifts. In the nonrelativistic DFT, the well-known linear dependency between experimental isomer shifts δ and calculated electron densities at the iron nuclei ρ_0 was verified for the range of iron complexes investigated in this study (Figure 2a). The data were fitted according to eq 1 and show small errors and root-mean-square deviation (RMSD) values (Table 2). The ZORA calculations yielded distinctly increased electron densities at the iron nuclei ($\rho_0 \sim 15\,560$ au^{-3} instead of $\rho_0 \sim 11\,817$ au^{-3} in the nonrelativistic case), which are already close to the fully relativistic Dirac−Fock result on ^{57}Fe d^5 (15 703.951 au^{-3}).[56] Early studies on the influence of relativistic corrections on MB data have shown that nonrelativistic and relativistic electron densities at the iron nuclei are related by an almost constant factor ranging between 1.3 and 1.4.[57,58] This is in line with our results; the ZORA densities are related to the nonrelativistic densities by a factor of 1.32, which is remarkably constant for all of the investigated model systems. Consequently, fit parameters of similar quality were obtained from the ZORA calculations and from the nonrelativistic approach (Table 2). This finding underlines, on one hand, the potential of the ZORA approach for predicting accurate isomer shifts,[59] but shows, on the other hand, that there is no improvement in comparison to the nonrelativistic approach.

A comparison of our nonrelativistic fit parameters with those obtained in a previous study employing the same methods has revealed excellent agreement.[13] This shows that the fit parameters do not strongly depend on a certain training

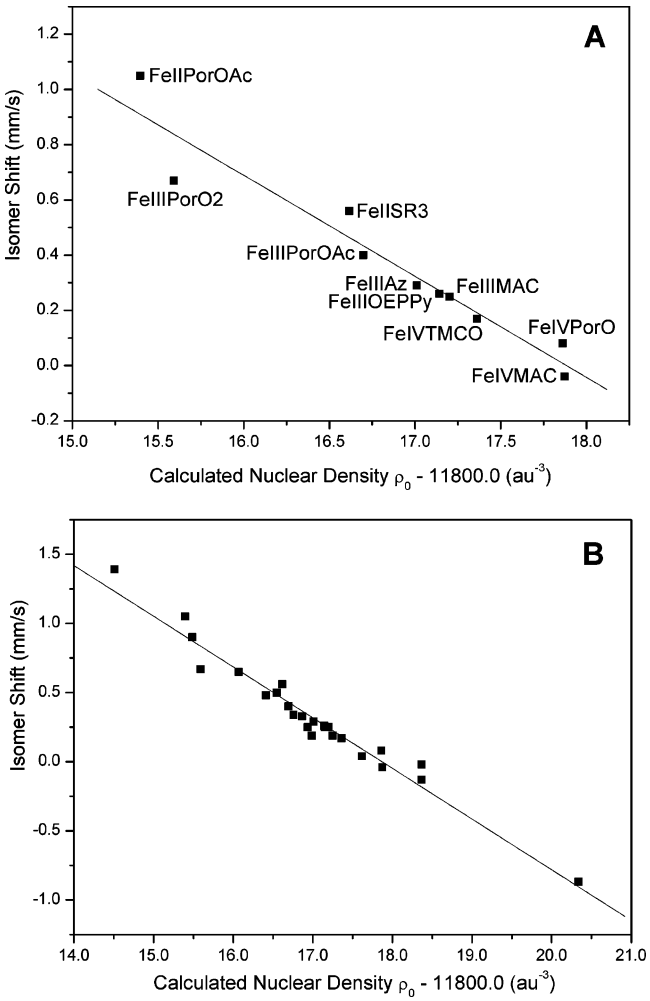

Figure 2. Linear relationship between experimental isomer shifts and calculated nuclear densities at the iron nuclei from nonrelativistic DFT (B3LYP). (**A**) Results from this study. (**B**) Combined results from this work and a previous study.[13]

(48) Eichkorn, K.; Weigend, F.; Treutler, O.; Ahlrichs, R. *Theor. Chem. Acc.* **1997**, *97*, 119−124.
(49) Eichkorn, K.; Treutler, O.; Ohm, H.; Häser, M.; Ahlrichs, R. *Chem. Phys. Lett.* **1995**, *240*, 283−289.
(50) The basis sets can be downloaded from the ftp server of the Turbomole home page at http://www.turbomole.com.
(51) Koseki, S.; Schmidt, M. W.; Gordon, M. S. *J. Phys. Chem.* **1992**, *96*, 10768−10772.
(52) Koseki, S.; Gordon, M. S.; Schmidt, M. W.; Matsunaga, N. *J. Phys. Chem.* **1995**, *99*, 12764−12772.
(53) Koseki, S.; Schmidt, M. W.; Gordon, M. S. *J. Phys. Chem. A* **1998**, *102*, 10430−10435.
(54) Neese, F. *ORCA—an Ab Initio, Density Functional and Semiempirical Program Package*, version 2.3; Max-Planck-Institut für Bioanorganische Chemie: Mülheim an der Ruhr, Germany, 2004.
(55) We have verified that our ZORA implementation exactly reproduces the data of van Lenthe and co-workers. Taking the HI molecule as an example, electric field gradients of 11.606 and 11.120 au^{-3} were calculated with the BP functional in ORCA, employing the ZORA and ZORA-4 densities, whereas values of 11.60 and 11.05 au^{-3} were reported in ref 38. For the Cu atom, isotropic hfcc's of 6748 and 6598 MHz were calculated with ORCA, employing the LSD and BP functionals, whereas values of 6750 and 6598 MHz were reported in ref 21. In all cases, large uncontracted, well-tempered Gaussian basis functions were used.
(56) Trautwein, A.; Harris, F. E.; Freeman, A. J.; Desclaux, J. P. *Phys. Rev. B: Condens. Matter* **1975**, *11*, 4101−4105.
(57) Desclaux, J. P. *Comput. Phys. Commun.* **1975**, *9*, 31−45.
(58) Mann, J. B. *J. Chem. Phys.* **1969**, *51*, 841−842.
(59) Zhang, Y.; Oldfield, E. *J. Phys. Chem. B* **2003**, *107*, 7180−7188.

Table 2. Fit Parameters α and β for the Linear Regression of Experimental Isomer Shifts (mm/s) and Calculated Electron Densities at the Iron Nuclei (au^{-3}) According to Eq 1

	NonRel[a]	NonRel[b]	NonRel[c]	ZORA[d]
C[e] (au^{-3})	11800.0	11800.0	11800.0	15550.0
α (au^3 mm/s)	-0.366 ± 0.036	-0.367 ± 0.017	-0.367 ± 0.015	-0.278 ± 0.028
β (mm/s)	6.54 ± 0.61	6.55 ± 0.29	6.55 ± 0.25	3.07 ± 0.28
R[f]	−0.96	−0.99	−0.98	−0.96
RMSD[g] (mm/s)	0.091	0.086	0.084	0.094

[a] Nonrelativistic results from this work (10 data points). [b] Nonrelativistic results from a different set of iron complexes (15 data points) employing similar methods.[13] [c] Combined data from both studies (25 data points). [d] Scalar relativistic results from this work (10 data points). [e] C is an arbitrary constant. [f] Correlation coefficient. [g] Root-mean-square deviation.

Table 3. Redetermined Nuclear Quadrupole Moment $Q(^{57}Fe)$ from B3LYP DFT Values

	NonRel	ZORA
$Q(^{57}Fe)$ (barn)	0.158 ± 0.014	0.156 ± 0.013

set of molecules and stimulated us to combine the calculated data of both computational studies. The results are even more accurate fit parameters with reduced errors and a smaller RMSD value (Table 2; Figure 2b).

Because a number of studies have tried to relate the MB experiments to MO descriptors such as the s population on the Fe center, we have also investigated the validity of such an approach. In our previous work, it was already shown that Löwdin s-orbital populations have no connection to the MB isomer shifts.[13] Here, we have extended these attempts to the natural populations analysis (NPA), which is clearly more sophisticated and of great value to the interpretation of chemical bonding.[60] However, in terms of the MB isomer shifts, the natural s populations show no discernible correlation with the experimental data. Consequently, no conclusion whatsoever can be drawn about MB properties of a given compound from the results of a NPA analysis.

Quadrupole Splittings. All of the investigated model systems show noncubic ligand and valence electron distributions. In consequence, nonzero ^{57}Fe electric field gradients were obtained throughout. Employing the calculated electric field gradients V and asymmetry parameters η, we plotted the experimental quadrupole splittings of all of the systems as a function of the calculated values of $^1/_2eV_z(1 + {}^1/_3\eta^2)^{1/2}$ (see eq 2). Linear fits of these data were used to redetermine the ^{57}Fe nuclear quadrupole coupling constant. From the nonrelativistic DFT and ZORA calculations, a similar value of $Q(^{57}Fe) \sim 0.16$ barn was obtained (Table 3), which is in very good agreement with the values that were reported and used in other studies (0.15−0.17 barn).[35,61−66] Employing the redetermined nuclear quadrupole moments, we give a comparison of calculated and measured quadrupole splittings in Figure 3. Correlation coefficients of 0.97 (NonRel) and 0.95 (ZORA) were obtained, whereas the RMSD values amount to 0.57 mm/s (NonRel) and 0.55 mm/s (ZORA). The high level of correlation for all of the model systems gives us confidence that the different oxidation states, charges, and ligand types have only a minor influence on the quality of the calculated data. Furthermore, the results show clearly that a nonrelativistic treatment of the electric field gradients is entirely satisfactory for ^{57}Fe despite the $\langle r^{-3} \rangle$ dependence of V, which would potentially seem to make the relativistic corrections, which are largest in the core region, mandatory.

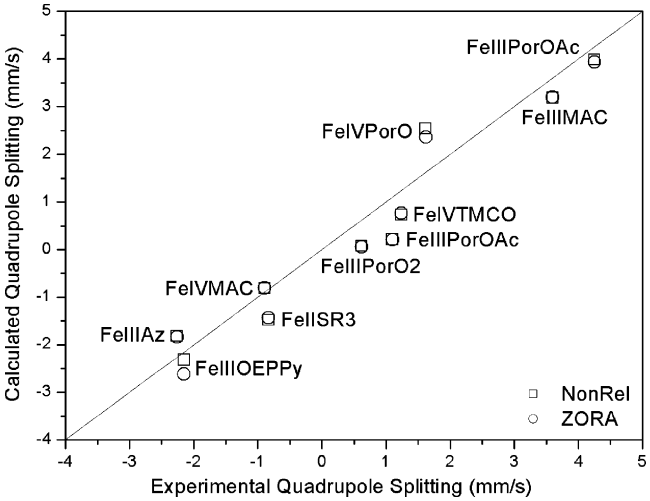

Figure 3. Comparison of calculated and measured ^{57}Fe quadrupole splittings. Nuclear quadrupole moments of 0.158 barn (nonrelativistic DFT) and 0.156 barn (ZORA) were used in the calculations.

Magnetic hfcc's. ^{57}Fe isotropic hfcc's A^{iso} of all of the investigated systems are given in Table 4 and Figure 4 in comparison to the experimental results. For most of the model systems, the typical underestimation of A^{iso} was found.[39,67,68] Furthermore, the RMSD values in Table 4 decrease with increasing computational levels; the scalar relativistic ZORA model, as well as the inclusion of spin−orbit effects, leads to an improvement of the calculated ^{57}Fe isotropic hfcc's (recall that, in the last case, A^{iso} refers to the sum of the Fermi contact term and the isotropic part of the SOC). The best agreement between theory and experiment was found in the ZORA calculations including SOCs (ZORA

(60) Glendening, E. D.; Badenhoop, J. K.; Reed, A. E.; Carpenter, J. E.; Bohmann, J. A.; Morales, C. M.; Weinhold, F. *NBO 5.0*; Theoretical Chemistry Institute: University of Wisconsin, Madison, WI, 2001. http://www.chem.wisc.edu/~nbo5.
(61) Martinez-Pinedo, G.; Schwerdtfeger, P.; Caurier, E.; Langanke, K.; Nazarewicz, W.; Söhnel, T. *Phys. Rev. Lett.* **2001**, *8706*, 062701.
(62) Zhang, Y.; Gossman, W.; Oldfield, E. *J. Am. Chem. Soc.* **2003**, *125*, 16387−16396.
(63) Zhi, Z.; Guenzburger, D.; Ellis, D. E. *J. THEOCHEM* **2004**, *678*, 145−156.
(64) Zhang, Y.; Oldfield, E. *J. Phys. Chem. A* **2003**, *107*, 4147−4150.
(65) Dufek, P.; Blaha, P.; Schwarz, K. *Phys. Rev. Lett.* **1995**, *75*, 3545−3548.
(66) Lauer, S.; Marathe, V. R.; Trautwein, A. *Phys. Rev. A: At., Mol., Opt. Phys.* **1979**, *19*, 1852−1861.
(67) Munzarová, M. L.; Kaupp, M. *J. Phys. Chem. A* **1999**, *103*, 9966−9983.
(68) Sinnecker, S.; Neese, F.; Noodleman, L.; Lubitz, W. *J. Am. Chem. Soc.* **2004**, *126*, 2613−2622.

Table 4. Calculated ^{57}Fe Isotropic hfcc's (MHz) and Comparison with Experimental Results[a]

structure	2*S*	NonRel	NonRel + SOC	ZORA	ZORA + SOC	exptl
Fe^{II}PorOAc	4	−18.5	−16.1	−20.2	−17.8	−21.8[26]
Fe^{II}SR3	4	−16.5	−13.6	−17.7	−14.9	−14.9[27]
Fe^{III}Az	1	−15.4	−10.0	−16.7	−11.3	−13.47[29]
Fe^{III}OEPPY	1	−16.7	−8.9	−18.2	−10.5	−6.8[70,30]
Fe^{III}MAC	3	−7.0 (−12.7)	−5.8	−7.4 (−12.4)	−6.2	−15.4[31]
Fe^{III}PorOAc	5	−18.0 (−32.7)	−18.0	−19.6 (−33.1)	−19.7	−27.5[26]
Fe^{III}PorO2	5	−14.7 (−26.7)	−13.6	−16.1 (−27.2)	−15.1	−32.1[32]
Fe^{IV}TMCO	2	−11.2 (−20.2)	−11.2	−12.4 (−20.9)	−12.6	−20[33]
Fe^{IV}PorO	2	−14.1 (−25.5)	−14.7	−14.0 (−23.6)	−14.7	−25.2[34]
Fe^{IV}MAC	4	−10.8 (−19.7)	−10.6	−11.7 (−19.7)	−11.5	−20[31]
RMSD		9.29	9.23	8.88	8.40	

[a] The isotropic hfcc's refer to the Fermi contact terms (NonRel and ZORA) or to one-third of the sum of the principal eigenvalues of the total hyperfine tensor (NonRel + SOC, ZORA + SOC, exptl). 2*S* is the number of unpaired electrons. For all of the complexes with small SOC contributions, Fermi contact terms that were scaled by factors of 1.81 (NonRel) and 1.69 (ZORA) are given in parentheses.

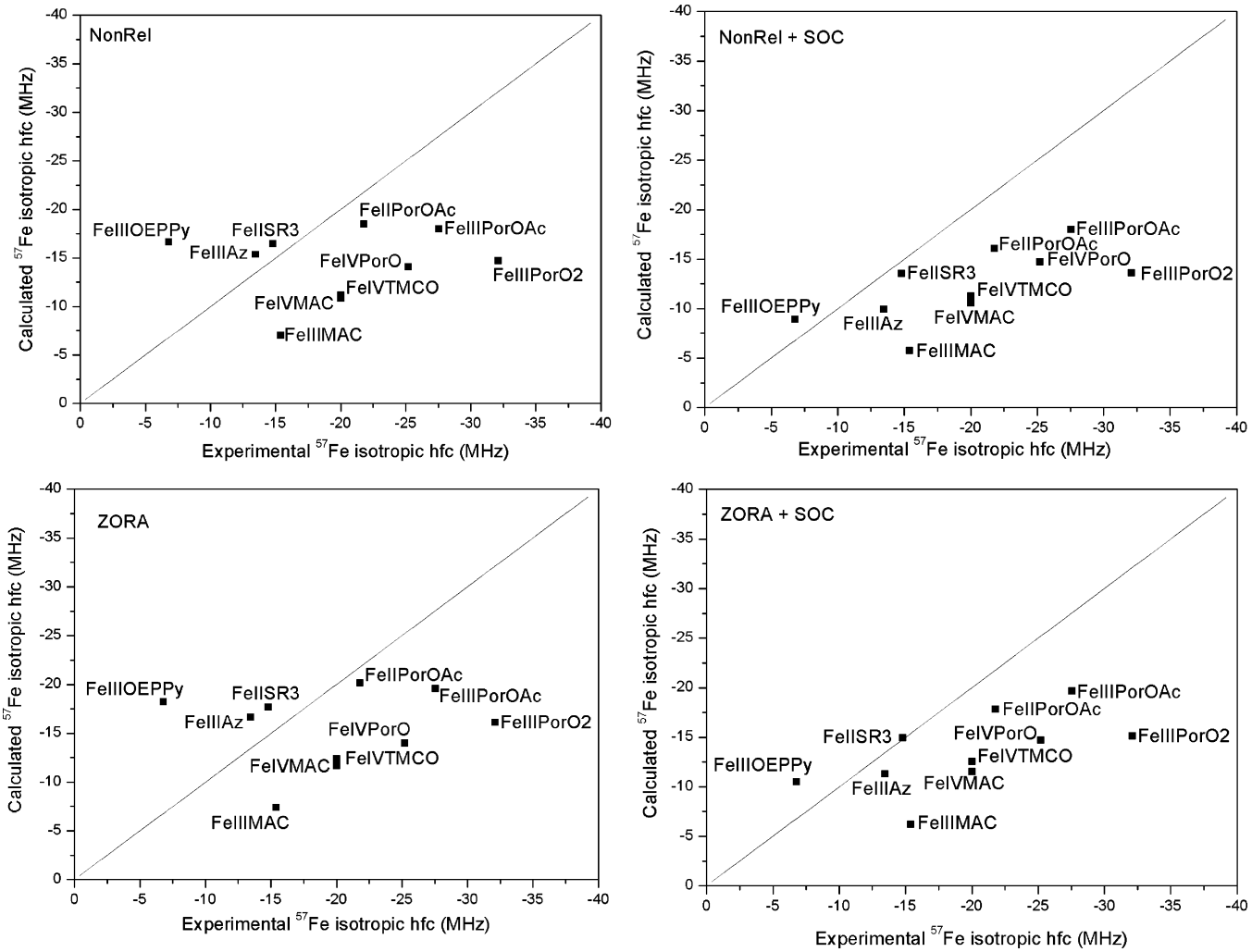

Figure 4. Comparison of calculated and measured ^{57}Fe isotropic hfcc's.

+ SOC). The magnitudes of changes introduced by the ZORA approach are typically in the range of 1−2 MHz, whereas the SOCs differ strongly depending on the systems. The deviations between theory and experiment are, in some cases, smaller than 20% (e.g., Fe^{II}PorOAc, Fe^{II}SR3, and Fe^{III}Az) but sometimes remain significant (up to 60% for Fe^{III}OEPPY and Fe^{III}MAC). They can be systematized with the aid of ligand field theory: The largest SOC effects were obtained for the low-spin ferric model systems ($S = {}^1/_2$), followed by those of the high-spin ferrous model systems ($S = 2$), both of which show nearly orbitally degenerate ground states. In these cases, the SOCs introduce changes to the isotropic hfcc's ranging from 10−50% and reasonable agreement between theory and experiment was found. Almost negligible SOCs were calculated for the high-spin ferric ($S = {}^5/_2$) and ferryl model systems ($S = 1$ or 2). For these systems, an underestimation of the isotropic hfcc's is evident (see Table 4). The computed hfcc's underline the importance of the inclusion of SOCs in the calculation of metal hyperfine tensors, as it was found in recent validation studies.[39,69]

Table 5. Fit Parameters for the Estimation of ^{57}Fe Isotropic hfcc's from Calculated Spin Densities at the Iron Nuclei in Complexes with Small SOCs (See Eq 13)

	NonRel	ZORA
α (MHz au^3)	131 ± 8	122 ± 8
R	0.86	0.86
RMSD	3.55	3.66

The good agreement between calculated (NonRel + SOC and ZORA + SOC) and measured isotropic hfcc's for the model systems with large SOCs (Fe^{II}PorOAc, Fe^{II}SR3, Fe^{III}Az, and Fe^{III}OEPPy) and the systematic underestimation of the isotropic hfcc's of all of the remaining complexes with small SOCs lead us to the following conclusions: (i) There is a general underestimation of the negative isotropic Fermi contact terms in all of the investigated systems. (ii) There is a general underestimation of the positive SOC contributions. In consequence, the calculated isotropic hfcc's are too small for all of the systems with small SOC contributions, whereas an error compensation occurs for all of the complexes with large SOCs, as has been discussed previously.[39]

For the first group of systems with small SOC contributions, fit parameters with rather small errors were obtained for the estimation of A^{iso} from calculated spin densities at the iron nuclei ρ_0^s:

$$A_{iso}^{est} = \alpha \frac{\rho_0^s}{S} \tag{13}$$

The obtained fit parameters from the nonrelativstic DFT and ZORA calculations are given in Table 5.

The determined fit parameters α can also be converted into scaling factors for the application on the calculated isotropic hfcc's:

$$A_{iso}^{est} = f A_{iso}^{calc} \tag{14}$$

The parameters f were obtained from

$$f = \frac{3\alpha}{4\pi P_A} \tag{15}$$

The results are factors of $f = 1.81$ for the nonrelativistic approach and $f = 1.69$ for the ZORA calculations. When these scaling factors are applied to the computed Fermi contact terms of all of the iron complexes with small SOCs (Fe^{III}MAC, Fe^{III}PorOAc, Fe^{III}PorO2, Fe^{IV}TMCO, Fe^{IV}PorO, and Fe^{IV}MAC) and the calculated A^{iso} values (NonRel + SOC and ZORA+SOC) are used for all of the complexes with large SOCs *without fitting* (Fe^{II}PorOAc, Fe^{II}SR3, Fe^{III}Az, and Fe^{III}OEPPy), good agreement between theory and experiment can be achieved for all of the model systems (Figure 5). The obtained RMSD values of 3.37 MHz (NonRel) and 3.19 MHz (ZORA) are distinctly smaller than the RMSD values reported in Table 4 (8−9 MHz).

A comparison of anisotropic ^{57}Fe hfcc's with the the experimental results shows very good agreement between theory and experiment for the ferryl complexes, whereas

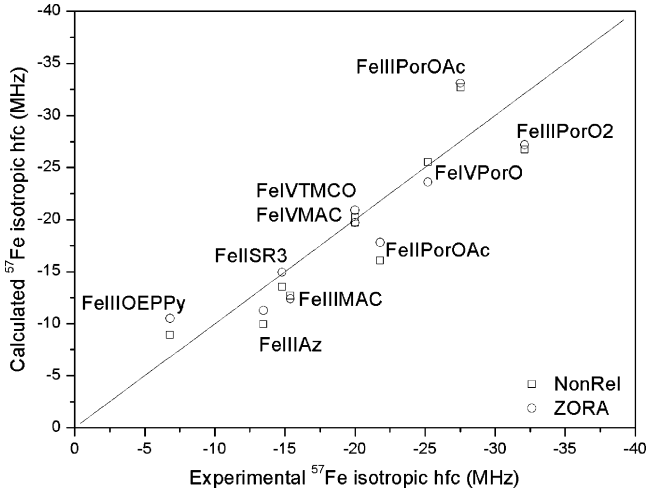

Figure 5. Comparison of theoretical and experimental ^{57}Fe isotropic hfcc's (MHz). For Fe^{II}PorOAc, Fe^{II}SR3, Fe^{III}Az, and Fe^{III}OEPPy, the A^{iso} values refer to the original DFT results including SOCs. For the remaining systems, the isotropic hfcc's were estimated by scaling the calculated Fermi contact terms with factors of 1.81 (NonRel) and 1.69 (ZORA).

Table 6. Calculated ^{57}Fe Anisotropic Hyperfine Data (MHz) and Comparison with Experimental Results

		NonRel	NonRel + SOC	ZORA	ZORA + SOC	exptl[a]
Fe^{II}PorOAc	A_1^{aniso}	−5.3	−5.5	−5.2	−5.5	−1.7
	A_2^{aniso}	−5.2	−4.8	−5.1	−4.7	−1.7
	A_3^{aniso}	+10.5	+10.3	+10.3	+10.1	+3.4
Fe^{II}SR3	A_1^{aniso}	+4.7	+6.2	+4.6	+6.1	+7.3
	A_2^{aniso}	+4.7	+6.2	+4.7	+6.1	+7.3
	A_3^{aniso}	−9.4	−12.3	−9.3	−12.2	−14.6
Fe^{III}Az	A_1^{aniso}	+19.7	+23.9	+19.5	+23.9	+16.6
	A_2^{aniso}	+14.6	+9.3	+14.5	+9.0	+4.8
	A_3^{aniso}	−34.3	−33.2	−34.0	−32.8	−21.5
Fe^{III}OEPPy	A_1^{aniso}	−32.6	−28.9	−32.4	−28.8	−50.5
	A_2^{aniso}	+12.7	+5.0	+12.6	+5.1	−17.6
	A_3^{aniso}	+20.0	+23.9	+19.8	+23.8	+68.2
Fe^{III}MAC	A_1^{aniso}	+25.0	+23.8	+24.9	+23.7	+22.3
	A_2^{aniso}	−15.7	−16.1	−15.6	−16.0	−14.9
	A_3^{aniso}	−9.3	−7.7	−9.3	−7.7	−7.4
Fe^{III}PorOAc	A_1^{aniso}	+0.4	+0.5	+0.3	+0.4	0.0
	A_2^{aniso}	−0.5	−0.7	−0.5	−0.6	0.0
	A_3^{aniso}	+0.1	+0.2	+0.1	+0.2	0.0
Fe^{III}PorO2	A_1^{aniso}	+1.7	+1.8	+1.6	+1.8	0.0
	A_2^{aniso}	+1.9	+2.0	+1.7	+1.9	0.0
	A_3^{aniso}	−3.5	−3.8	−3.4	−3.7	0.0
Fe^{IV}TMCO	A_1^{aniso}	−7.4	−8.0	−7.4	−8.0	−11
	A_2^{aniso}	−6.8	−7.7	−6.9	−7.8	−5
	A_3^{aniso}	+14.3	+15.7	+14.3	+15.8	+16
Fe^{IV}PorO	A_1^{aniso}	−11.1	−11.2	−9.1	−9.4	−9.2
	A_2^{aniso}	−6.1	−6.7	−8.0	−8.6	−9.2
	A_3^{aniso}	+17.2	+17.9	+17.1	+17.9	+18.3
Fe^{IV}MAC	A_1^{aniso}	−3.8	−3.6	−3.8	−3.6	−4.7
	A_2^{aniso}	−1.2	−0.8	−1.3	−0.9	−0.6
	A_3^{aniso}	+5.0	+4.4	+5.1	+4.5	+5.3

[a] See Table 4 for references.

good agreement was found for the ferrous and ferric complexes (Table 6). Taking the Fe^{II}PorOAc complex as an example, the experimental anisotropy of the A tensor of the ferrous ion, as reported by Bominaar et al.,[26] was overestimated in the calculations. The same study revealed an isotropic ^{57}Fe A tensor in the ferric species that was well-recovered in the calculations on Fe^{III}PorOAc. A more detailed discussion of the anisotropic ^{57}Fe hfcc's shows that the ZORA corrections are mostly small (∼0.1 MHz) but can approach ∼2 MHz and improve the agreement with the

(69) Arbuznikov, A. V.; Vaara, J.; Kaupp, M. *J. Chem. Phys.* **2004**, *120*, 2127−2139.

Table 7. Comparison of Calculated and Measured Spectroscopic Data of the $[Fe(H_2O)_6]^{3+}$ Ion

	NonRel	ZORA	exptl[25]
δ (mm/s)	0.60	0.63	0.51
ΔE_Q (mm/s)	0.00	0.00	0.0
A_{iso}^{est} (MHz)	−35.8	−36.7	−32.6

experiment. The SOC contributions are distinctly larger than the scalar relativistic corrections for the majority of the investigated iron complexes. They can easily exceed 20% (e.g., for Fe^{II}SR3, Fe^{III}Az, and Fe^{III}OEPPy). Considering Fe^{II}SR3 as an example, the inclusion of SOC contributions leads to a noticeably better agreement between theory and experiment.

The High-Spin $[Fe(H_2O)_6]^{3+}$ Ion. In addition to the 10 iron complexes from Figure 1, calculations were performed on the high-spin ferric $[Fe(H_2O)_6]^{3+}$ species as an application case. The isomer shifts were calculated from the electron densities at the iron nuclei employing the fit parameters from Table 2. Quadrupole splittings were calculated applying the ^{57}Fe nuclear quadrupole moments from Table 3. The ^{57}Fe hyperfine tensor of $[Fe(H_2O)_6]^{3+}$ is dominated by the Fermi contact term, whereas negligible dipolar hyperfine and SOC contributions were calculated. The computed Fermi contact terms (−19.78 MHz from NonRel and −21.72 MHz from ZORA) were scaled with factors of 1.81 (NonRel) and 1.69 (ZORA). A comparison of the calculated and experimental results is given in Table 7.[25] The almost ideal octahedral coordination of the metal ion (R_{Fe-O} = 2.068 Å) leads to vanishing quadrupole splittings in both experiments and calculations. The experimental isomer shift and the isotropic hfcc were somewhat overestimated in the calculations. However, data of similar quality were obtained for the high-spin ferric model complexes from Table 1 (Fe^{III}PorOAc and Fe^{III}PorO2), which underlines the transferability of this work to other iron complexes.

5. Summary and Conclusions

In the present work, electric and magnetic hyperfine parameters of 10 iron complexes, which cover a wide range of oxidation and spin states and ligand types, were calculated employing DFT.

The linear relationship between calculated electron densities at the iron nuclei and experimental isomer shifts was shown to be valid for this set of model systems. Although it is well-known that the obtained fit parameters noticeably depend on the chosen computational method, a comparison of our work with other results[13] has revealed that there is only a weak dependency of the fit parameters on the specific training set. This makes the development of more universal calibration constants possible. Fit parameters of similar accuracy were obtained employing nonrelativistic and quasi-relativistic DFT methods. The ZORA densities are shifted by a factor of 1.32, upward in the direction of the four-component Dirac−Fock limit, but the correlation with the experiment does not improve at the same time. From a comparison of calculated electric field gradients at the iron nuclei and experimental quadrupole splittings, the ^{57}Fe nuclear quadrupole moment was redetermined to a value of ∼0.16 barn (nonrelativistic DFT and ZORA). The calculated quadrupole splittings show good agreement with the experimental results; scalar relativistic ZORA calculations give no improvement in comparison to the nonrelativistic calculations. Obviously, the chemical trends in the quadrupole splittings and isomer shifts originate from the valence shells, which are little affected by relativity. The situation is different, however, for systems with large SOC contributions and for heavy elements.[24,71] Similar small relativistic effects in the calculation of quadrupole splittings were found by Zhang and Oldfield, whom employed the ZORA and the Pauli formalisms.[59]

The high potential of DFT methods for the prediction of ^{57}Fe isomer shifts and quadrupole splittings, which was demonstrated already for five- and six-coordinate iron porphyrins,[62,72,73] iron phthalocyanines,[74] and two- and three-coordinate Fe^{II} and Fe^{III} complexes,[59,75] as well as for biological systems,[73,76−79] was fully confirmed in this work for all 10 of the investigated model complexes, which are partly unique in their class.

The accurate calculation of ^{57}Fe isotropic hfcc's turned out to be more complicated. However, the apparently widely scattering results, in comparison to those of the experimental data, could be traced back to the effect of spin−orbit coupling. For systems with small SOC contributions, the experimental isotropic hfcc's were systematically underestimated by factors of 1.81 (nonrelativistic DFT) and 1.69 (ZORA), which also demonstrates the improvement of the results by the scalar relativistic approach. In contrast and somewhat surprisingly, the best agreement between calculated isotropic hfcc's and experimental data was achieved for the more complicated systems with large SOCs (Fe^{III} with $S = {}^1/_2$, Fe^{II} with $S = 2$), where the pseudocontact shift can easily change the isotropic hfcc's by 10−50%. In these cases, the good agreement between theory and experiment must be attributed to an error cancellation, that is, a considerable underestimation of the SOC effect together with too-positive values for the Fermi contact contributions.[39] The underestimation of the SOC contributions is particularly evident in the calculated g shifts, which are considerably in error (Supporting Information). In addition, accurate ^{57}Fe anisotropic hfcc's were calculated in this work. Here also, the

(70) Benda, R.; Schunemann, V.; Trautwein, A. X.; Cai, S.; Polam, J. R.; Watson, C. T.; Shokhireva, T. K.; Walker, F. A. *J. Biol. Inorg. Chem.* **2003**, *8*, 787−801.
(71) van Lenthe, E.; van der Avoird, A.; Hagen, W. R.; Reijerse, E. J. *J. Phys. Chem. A* **2000**, *104*, 2070−2077.
(72) Smith, D. M. A.; Dupuis, M.; Vorpagel, E. R.; Straatsma, T. P. *J. Am. Chem. Soc.* **2003**, *125*, 2711−2717.
(73) Zhang, Y.; Mao, J. H.; Godbout, N.; Oldfield, E. *J. Am. Chem. Soc.* **2002**, *124*, 13921−13930.
(74) Nemykin, V. N.; Kobayashi, N.; Chernii, V. Y.; Belsky, V. K. *Eur. J. Inorg. Chem.* **2001**, 733−743.
(75) Andres, H.; Bominaar, E. L.; Smith, J. M.; Eckert, N. A.; Holland, P. L.; Münck, E. *J. Am. Chem. Soc.* **2002**, *124*, 3012−3025.
(76) Han, W. G.; Lovell, T.; Liu, T. Q.; Noodleman, L. *Inorg. Chem.* **2003**, *42*, 2751−2758.
(77) Oldfield, E. *Annu. Rev. Phys. Chem.* **2002**, *53*, 349−378.
(78) Lovell, T.; Li, J.; Liu, T. Q.; Case, D. A.; Noodleman, L. *J. Am. Chem. Soc.* **2001**, *123*, 12392−12410.
(79) Vrajmasu, V.; Münck, E.; Bominaar, E. L. *Inorg. Chem.* **2003**, *42*, 5974−5988.

ZORA method and the inclusion of second-order contributions lead to more accurate data. To the best of our knowledge, such a detailed comparison of ^{57}Fe hyperfine data of different iron complexes from DFT has not been given outside of this paper. However, the outstanding work of Noodleman and co-workers already provided an in-depth understanding of the ^{57}Fe hyperfine data of iron−sulfur clusters.[80−82]

Finally, calculations were performed on the $[Fe(H_2O)]^{3+}$ ion as an application case; that is, the fit parameters from this work were used for the calculation of its spectroscopic data. A comparison with measured data showed good agreement between theory and experiment.

The thorough application of computational methods to experimentally well-investigated systems is a prerequisite to the investigation of less well-understood or short-lived species. In this respect, the present study has shown that accurate calculations of isomer shifts, nuclear quadrupole splittings, and, to a certain extent, magnetic hyperfine data were possible for all of the investigated iron oxidation and spin states. The obtained information should be highly transferable to other theoretical studies on inorganic iron complexes and biological systems, as will be demonstrated in forthcoming application studies.

Acknowledgment. This work has been supported by the priority program 1137 "Molecular Magnetism" (F.N.) and the Max-Planck Gesellschaft.

Supporting Information Available: Calculated electron densities at the iron nuclei and isomer shifts of all of the complexes obtained from the fit parameters in Table 2, the relationship between ^{57}Fe natural s populations and experimental isomer shifts, a comparison of calculated and measured ^{57}Fe quadrupole splittings, the relationship between experimental ^{57}Fe isotropic hfcc's and calculated spin densities for all of the model systems with small SOCs, and a comparison of calculated and measured *g* tensors. This material is available free of charge via the Internet at http://www.pubs.acs.org.

IC048609E

(80) Mouesca, J. M.; Noodleman, L.; Case, D. A.; Lamotte, B. *Inorg. Chem.* **1995**, *34*, 4347−4359.
(81) Mouesca, J. M.; Noodleman, L.; Case, D. A. *Inorg. Chem.* **1994**, *33*, 4819−4830.
(82) Noodleman, L. *Inorg. Chem.* **1991**, *30*, 246−256.